Energy Technology
Generation, Conversion, Storage, Distribution
www.entechnol.de

A Sodium Polysulfide Battery with Liquid/Solid Electrolyte: Improving Sulfur Utilization Using P_2S_5 as Additive and Tetramethylurea as Catholyte Solvent

*Lukas Medenbach, Pascal Hartmann, Juergen Janek, Timo Stettner, Andrea Balducci, Cornelius Dirksen, Matthias Schulz, Michael Stelter, and Philipp Adelhelm**

Herein, the proof of concept of a sodium polysulfide battery consisting of two electrode chambers being separated by a solid electrolyte is described. The concept is suited for dissolved polysulfide cathodes and has the advantage that both half reactions can be optimized separately. The formation of solid sulfide discharge products is identified as the major limiting factor for cell cycling. This issue can be alleviated by adding solid P_2S_5. Further improvement can be achieved by replacing diglyme (2G) as the cathode compartment solvent with tetramethylurea (TMU). Using TMU, the cell cycles with Coulombic efficiencies >99% and capacities of 800 mAh g^{-1} are maintained for at least 30 cycles. Viscosity, density, conductivity, and the electrochemical stability window values of the 2G- and TMU-based electrolytes are compared. The latter shows higher viscosity (2.806 vs 1.603 mPa s), higher density (1.016 vs 0.996 g cc^{-1}), and higher conductivity (4.27 vs 1.45 mS cm^{-1}). The oxidative stability limit of the TMU electrolyte is 3.2 V versus Na^+/Na, which is sufficient for polysulfide redox reactions. Vis spectroscopy is used to follow the electrode reaction. In case of TMU, the reaction is based on the redox activity of $S_3^{-\bullet}$ radicals (blue coloration of the catholyte solution).

1. Introduction

Rechargeable metal–sulfur batteries are attractive energy storage systems due to their high theoretical energy density and the abundance of sulfur. The most advanced concepts are the lithium–sulfur battery (operating at ambient conditions) and the high-temperature sodium–sulfur (NaS) battery operating at about 300 °C. The NAS battery concept is based on liquid electrodes being separated by a solid electrolyte. During discharge, sodium ($\vartheta_m = 98$ °C) reacts with sulfur ($\vartheta_m = 119$ °C) to form molten polysulfides (Na_2S_x, $x \approx 3$). The anode and cathode are separated by a sodium ion–conducting ceramic membrane known as Na-β″-aluminate. The NAS battery has been commercialized by NGK Insulators (Aichi, Japan) for stationary energy storage but the operating temperature of around 300 °C is technologically challenging and has led to safety concerns in the past.[1]

Nevertheless, the use of sodium and sulfur as active materials in batteries is very appealing as both elements are abundant which may lead to cost-effective batteries. Considering this, lowering the operating temperature of NaS batteries, potentially down to room temperature, became an attractive research field in the past years.[2] The redox chemistry of sulfur is, however, very complex, and its use in rechargeable batteries operating at room temperature could

L. Medenbach, T. Stettner, Prof. A. Balducci, Prof. P. Adelhelm
Institute of Technical Chemistry and Environmental Chemistry (ITUC)
Center for Energy and Environmental Chemistry (CEEC Jena)
Friedrich-Schiller-University Jena
Philosophenweg 7a, 07743 Jena, Germany
E-mail: philipp.adelhelm@hu-berlin.de

Dr. P. Hartmann
Digitalization - Battery Materials and Inorganics
BASF SE
Carl Bosch Straße 38, 67056 Ludwigshafen, Germany

The ORCID identification number(s) for the author(s) of this article can be found under https://doi.org/10.1002/ente.201901200.

DOI: 10.1002/ente.201901200

Dr. P. Hartmann, Prof. J. Janek
Institute of Physical Chemistry & Center for Materials Research
Justus-Liebig-University Giessen
Heinrich-Buff-Ring 17, 35392 Giessen, Germany

C. Dirksen, Dr. M. Schulz, Prof. M. Stelter
Stationary Energy Storage
Fraunhofer Institute for Ceramic Technologies and Systems (IKTS)
Michael Faraday Straße 1, 07629 Hermsdorf, Germany

Prof. P. Adelhelm
Institute of Chemistry
Humboldt University of Berlin
Brook-Taylor-Str. 2, 12489 Berlin, Germany

Prof. P. Adelhelm
Helmholtz-Zentrum Berlin für Materialien und Energie (HZB)
Albert-Einstein-Str. 15, 12489 Berlin, Germany

not be satisfactorily optimized to date. Most experience is available for the lithium–sulfur battery, and the related challenges have been extensively reviewed in the past.[2b,3] The same fundamental challenges also apply to other metal–sulfur batteries (Na, K, or Mg), though to different degrees.[4] Very briefly, the challenges relate to 1) the insulating properties of solid sulfur and sulfide phases which require adding substantial amounts of conductive support material, 2) the volume expansion during discharge (+70% for $S \rightarrow Li_2S$ and +180% for $S \rightarrow Na_2S$), 3) the solubility of polysulfide intermediates (S_x^{2-}, $S_3^{-\bullet}$), causing the cell reaction to be a combined dissolution/precipitation process and causing a chemical short circuit of the cell (shuttle mechanism), and 4) the common challenges of metal electrodes (dendrite formation and electrolyte consumption) along with the side reactions occurring with the dissolved polysulfides.

Moreover, the reaction might be further complicated by a "sulfur spillover" process as we reported recently.[5]

Considering the high solubility of polysulfides in many solvents, it may therefore appear more promising to adopt an alternative cell concept, i.e., using a dissolved sulfur cathode. Here, only dissolved polysulfides ($Na_2S_x^{2-}$) are cycled, whereas solid sulfides such as Na_2S are generally avoided, and hence issues related to their insulating properties as well as the volume expansion are eliminated or at least alleviated. Such a concept was proposed as early as 1978 by Abraham et al.[6] The cell concept consists of two separate electrode chambers (anode and cathode compartments) with liquid electrolytes that are separated by a Na^+ selective membrane such as Na-β″-aluminate[7] or Nafion-like polymers.[8] The cell concept is shown in **Scheme 1**a. The concept may also allow raising the operating temperature above the melting point of sodium. Such an "intermediate-temperature" Na/S battery has the benefits of avoiding dendrite formation and eliminates the need for a liquid electrolyte in the anode compartment.[6a,9] As the system's capacity is usually limited by the solubility of the polysulfides, aqueous catholytes in combination with water-stable membranes made of LISICON were tested.[10] Despite the advantages of high polysulfide solubility, the combination of aqueous electrolytes and molten sodium in a battery is likely of too high risk.

While the concept of a dissolved sulfur cathode with a solid electrolyte as a separating membrane increases the complexity for efficient ion transfer,[11] a specific advantage is that each liquid electrolyte is only in contact with one electrode. This means that the electrolyte composition can be optimized separately for each electrode reaction. This liquid/solid/liquid electrolyte configuration is quite different from conventional batteries in which the liquid electrolyte is in contact with the anode and the cathode and hence must show sufficient reductive/oxidative stability with both of them.

In this study, we use the cell concept shown in Scheme 1a for realizing a NaS battery operating at room temperature. A major problem of a dissolved sulfur cathode concept is the evolution of sulfide precipitates and their reactivation during charging.[12] We therefore discuss two different strategies on how to increase sulfur utilization and rechargeability. First, P_2S_5 is used as an additive which improves the dissolution and reactivation of precipitated sulfides.[13] Second, tetramethylurea (TMU) is used as an alternative solvent for the catholyte mixture. Results are compared with a reference system based on diglyme (2G), as the solvent class of ethers is commonly applied in metal–sulfur battery research. We further apply vis spectroscopy to gain information on the state of charge (SOC) as well as the nature of polysulfide intermediates. Finally, we also discuss the present challenges of this cell concept.

2. Results and Discussion

2.1. The Na Polysulfide Cell: Cycling and Failure

We used a transparent, tubular glass container (200 mL) for the cell construction, see Scheme 1b. The use of glass provides a convenient way to visibly follow the reaction of the dissolved sulfur cathode during charging/discharging. In a first set of

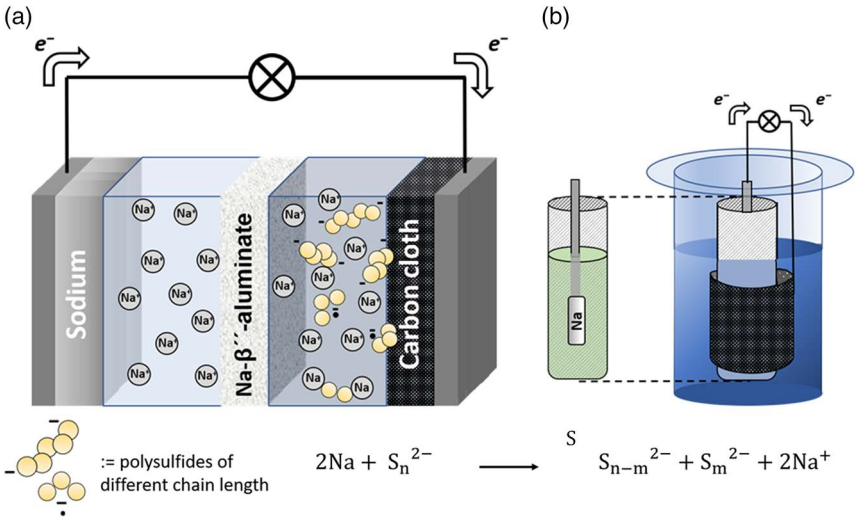

Scheme 1. a) Na polysulfide cell concept with two electrolyte chambers separated by a sodium-ion selective membrane. b) Lab-scale Na polysulfide cell used in this work. A more detailed cell setup description can be found in Figure S1, Supporting Information. In both illustrations, the electron flow represents the discharge process. Excess of positive charges is compensated by triflate (OTf^-) counter ions (not shown in the scheme).

experiments, the cathode compartment consisted of a 2G-based catholyte containing dissolved Na_2S_4 (5 mM) and Na-trifluoromethanesulfonate (NaOTf, 0.25–0.5 M). The higher concentration of NaOTf compared with Na_2S_4 ensures a constant conductivity during cell cycling and eases the optical characterization. A carbon gas diffusion layer (GDL) served as a current collector. Dissolution of Na_2S_4 in the electrolyte solution was rapid, and a deep green colored solution was obtained in just a few seconds. The same coloration is also observed for the mono- and tetraglyme ethers (1G, 4G). For the anode compartment, sodium metal was pressed on a cylindrical stainless-steel current collector, which was immersed in a solution of NaOTf in 2G (0.25–0.5 M). The choice of NaOTf/2G as electrolyte solution is motivated because of its good stability and low interface resistance compared with other electrolyte solutions.[14] Despite these advantages, it is of note that dendrite formation remains an issue,[15] see Figure S2, Supporting Information.

Galvanostatic discharging occurs at around 1.7 V (22 °C), see **Figure 1**, though only a limited capacity was achieved at a current of 0.01 C (≈500 µA). The poor sulfur utilization could be partially alleviated by catholyte stirring and increasing the temperature to 50 °C which led to a discharge voltage of around 2 V. Gradual reduction of the polysulfide solution should lead to short-chain sulfides, followed by precipitation of insoluble sulfides. This trend could be directly followed in the glass cell, i.e., discoloration and precipitation took place. The achieved capacity was 570 mAh g_S^{-1}, indicating that Na_2S_2 is the discharge product (1254 mAh g_S^{-1} would be expected in case of complete Na_2S formation).

Recharging of the cell, however, was barely possible despite the solution being continuously stirred. Obviously, the formation of insoluble sulfide precipitates is not desirable for the cell presented here. It is of note, however, that elemental sulfur exhibits sufficient carbon affinity and can be at least partially reduced without further treatment. Sulfide precipitation may be avoided by shallow cycling of the cell (e.g., by adjusting the lower cut-off potential). This approach indeed improved the rechargeability of the cell though cycle life was still poor, and the capacity yield was much lower compared with deep discharging, see Figure S3, Supporting Information. Overall, a more effective activation of sulfide precipitates is required to improve the reversible charge storage capacity of the cell. One strategy to overcome this problem is to use P_2S_5 as additive.

2.2. The Effect of P_2S_5 Additive

Phosphorous pentasulfide (P_2S_5) has been proposed as an additive by Lin et al. due to its ability to ease dissolution of otherwise insoluble lithium or sodium (poly-)sulfides by forming polysulfidophosphate complexes.[13,16] P_2S_5 and Na_2S on their own are insoluble in 2G but their combination results in a clear, yellow solution (Figure S4, Supporting Information). In our study, we adjusted the composition of polysulfide and P_2S_5 additives so as to reach a formal composition of Na_3PS_4. For this, a 2G-based solution containing 1 mM Na_2S_5 and 1.67 mM P_2S_5 was prepared. Stirring led to an almost transparent solution instead of a deep electrolyte coloration which would be expected for bare polysulfide solutions (Figure S5, Supporting Information). A speculative—lastly unproven—explanation would be that Na_2S_5 and P_2S_5 undergo chemical interactions, wherein phosphorous does not maintain its +V oxidation state. The S_5^{2-} anion, in contrast, might be oxidized to optically inactive sulfur. The detailed understanding of the solution chemistry after P_2S_5 addition is out of the scope of the current article but is definitely worth further in-depth investigation.

The effect of the additive is quite significant, leading to an initial discharge capacity of 1100 mAh g_S^{-1}, without any visible precipitation at room temperature (22 °C). Recharging was possible as well. The reduction and oxidation of sulfur can be followed by color changes of the catholyte, see **Figure 2**a. Voltage profiles of selected cycles are shown in Figure 2b, whereas Figure 2c shows summarizing charge capacities, discharge capacities, and Coulombic efficiencies of 30 cycles. Note that, we calculated the Coulombic efficiency by dividing the discharge capacity by the preceding charge capacity. Despite these promising results, the capacity fade was still strong. After 30 cycles, the capacity reached only 600 mAh g_S^{-1} and continued to fade. This suggests that 2G—as well as other commonly used glymes—may not be the best solvent for enabling long cycle life.

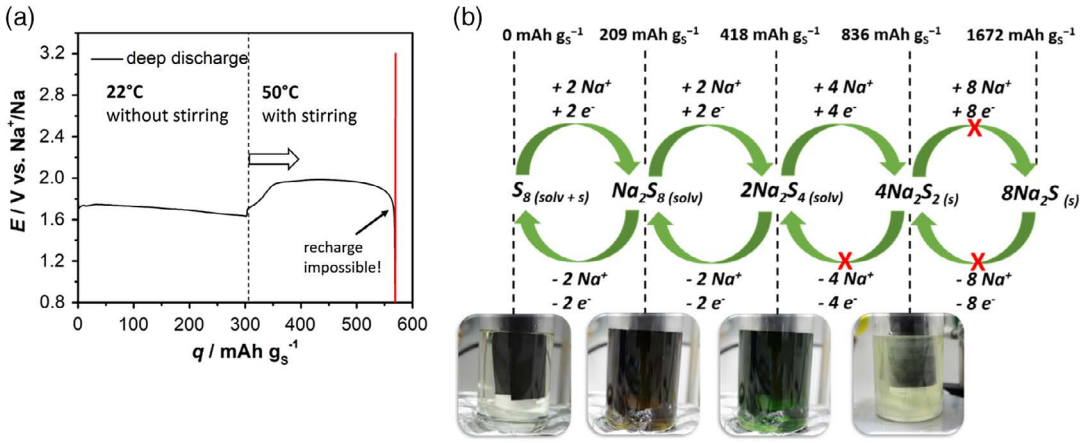

Figure 1. a) Slow deep discharge (0.01 C) of Na polysulfide cell with 2G catholyte and 2.5 mmol L^{-1} Na_2S_4. Recharging of the cell was not successful. b) Simplified scheme of polysulfide electrochemistry and sluggish reaction pathways (marked with a red cross) due to the conversion of precipitated sulfides. The photographs show the catholyte during discharging.

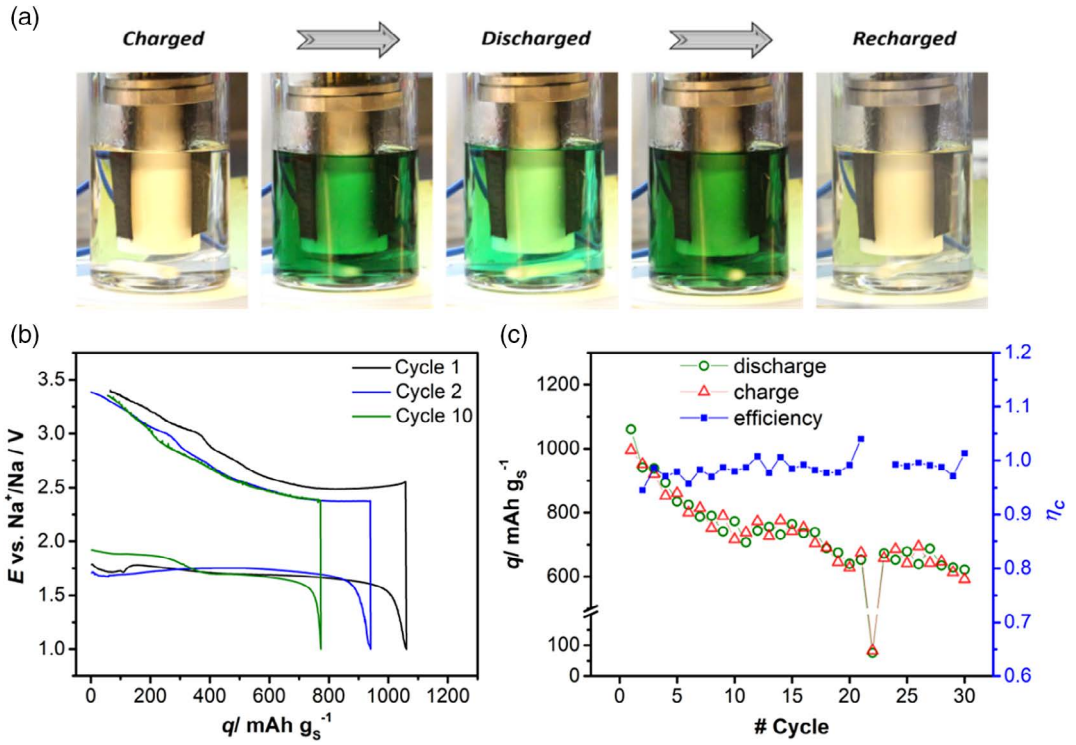

Figure 2. a) Appearance of Na polysulfide catholyte based on 2G solvent across a full discharge/charge cycle. b) Voltage profiles for cycle 1, 2, and 10 at a current rate of 0.083 C (60 μA cm^{-2}). c) Discharge capacities, charge capacities, and Coulombic efficiencies for the first 30 cycles at same *C* rate. Anolyte was 0.5 M NaOTf in 2G.

However, as sodium electrodes can be easily cycled in glyme-based electrolytes, it is likely that the limited cycle life of the cell is due to the glyme electrolyte on the cathode side. As discussed earlier, the cell concept with a separating solid electrolyte provides the opportunity to use different electrolytes for both electrodes. We therefore replaced the 2G solvent on the cathode side by another solvent. Among various solvents tested (dimethyl acetamide [DMAc], dimethoxy ethane [DME], and 4G) (Figure S6, Supporting Information), TMU appeared most promising and is discussed in more detail in the following section.

2.3. TMU as Catholyte + P_2S_5 Additive

TMU is a solvent that is hardly being applied in batteries. To the best of our knowledge, there is only one very recent report on using this solvent as electrolyte component for metal–sulfur batteries. Zhang et al. compared the performance of standard dioxolane/dimethoxyethane (DOL/DME)-based electrolytes (with $LiNO_3$ as the cosalt) with DOL/TMU and found a better performance, particularly, in terms of capacity utilization.[17] We chose to make use of TMU as the solvent due to its reported stability against sulfur[18] and its dielectric constant of 23.06–23.60,[19] which is higher compared with the glymes (7–8[20]), and therefore, TMU should be able to dissolve more (poly)sulfides. The physicochemical characterization (electrochemical stability window [ESW], conductivity, and viscosity) of the TMU electrolyte is discussed in Section 3. Following the results described in the previous section, we further added P_2S_5 with the same concentration to the TMU catholyte.

Figure 3 shows the cycling performance at 0.1 C for the cell with TMU as catholyte solvent along with photographs of the cell at various SOC. The first observation is that the solution is blue due to the presence of $S_3^{-\bullet}$ radicals, as it has been observed for dimethyl sulfoxide (DMSO)-based electrolytes as well.[21] The initial cycle shows a discharge capacity as high as 1200 mAh g_S^{-1} of which around 800 mAh g_S^{-1} can be recovered during charging. From this, one might also expect a rapid capacity fade just like in the case of 2G. However, the capacity loss stops after around ten cycles, followed by a slight increase to reach more than 800 mAh g_S^{-1}. The Coulombic efficiency also increased. Average values were 99.3% compared with 98.6% in the case of 2G. Note that few data points are missing because the cell was operated within a glovebox that was frequently also used for other experiments. This led to some singular events, see also cycle 22 in Figure 2c, which are not representative for the cell.

The rate capability (*C*-rate test) of the cell is shown in Figure 3c. Compared with 0.1 C, lowering the current did not increase the degree of sulfur utilization. Higher currents, however, led to a capacity decrease. At 0.2 C, about 550 mAh g_S^{-1} was achieved. In addition to diffusion limitation, the large voltage drop across the electrolyte volume is a major cause for the capacity loss at increasing currents because the cut-off potential is reached very early, particularly for rates >0.2 C.

2.4. Electrolyte Characterization

As stated earlier, TMU is an electrolyte solvent that is hardly applied in rechargeable batteries. This section therefore

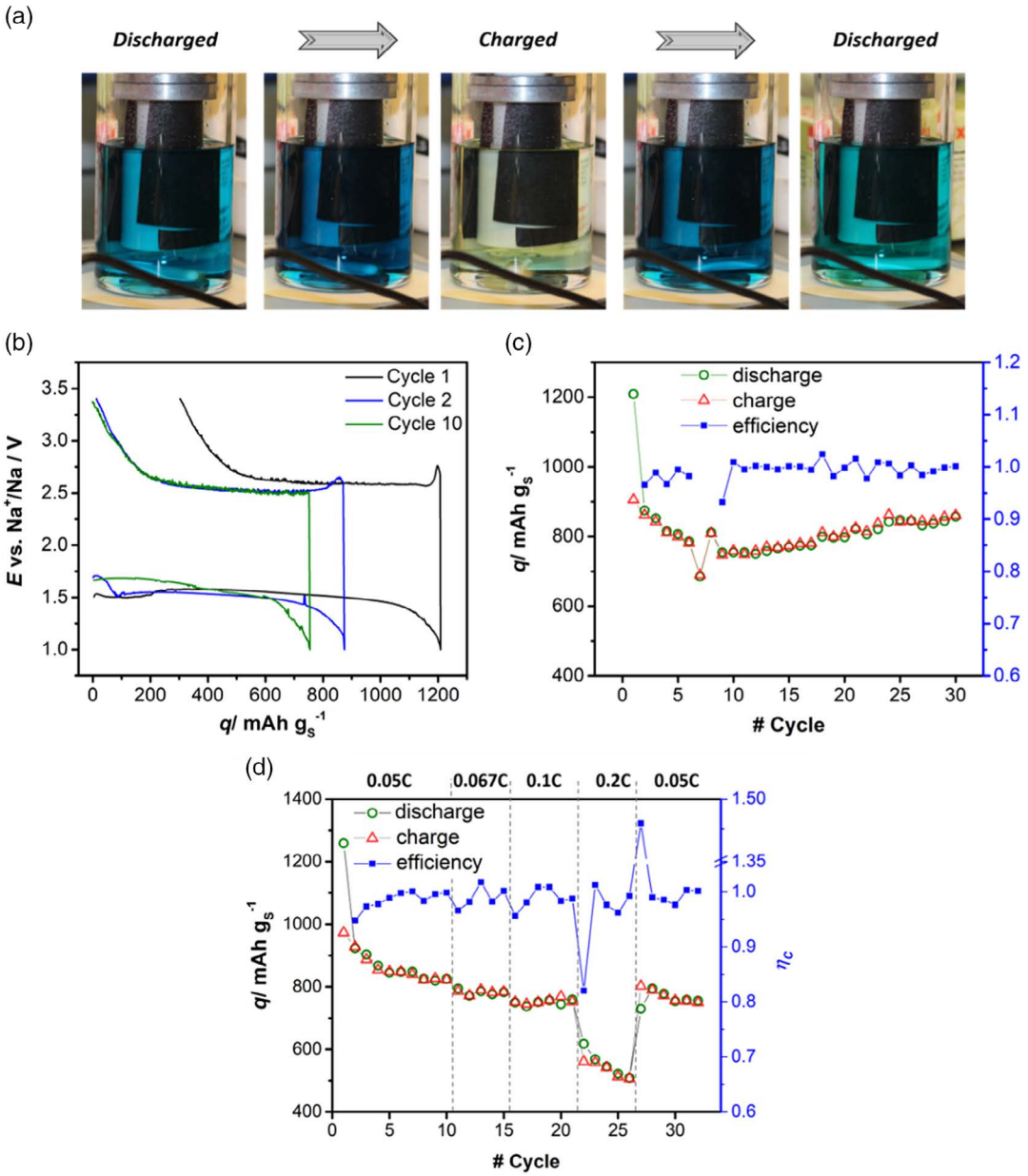

Figure 3. a) Appearance of Na polysulfide catholyte based on TMU solvent across a full charge/discharge cycle. b) Voltage profiles for cycle 1, 2, and 10 at a current rate of 0.1 (72 μA cm^{-2}). c) Discharge capacities, charge capacities, and Coulombic efficiencies for the first 30 cycles at same *C* rate. d) Rate performance test for additional *C* rates 0.05, 0.067, and 0.2 C. Further current increase resulted in performance collapse.

summarizes some basic physicochemical properties. Ionic conductivity, viscosity, density, and ESW of the 0.5 M NaOTf/TMU electrolyte were measured and compared with the 0.5 M 2G electrolyte. Except the ESW, all measurements were carried out as a function of temperature. Polysulfides were not added due to possible corrosion of some of the measurement setups.

At 20 °C the TMU electrolyte shows a total ionic conductivity of 4.3 mS cm^{-1} which is three times higher compared with the 2G electrolyte, see **Figure 4**a. With increasing temperature, the conductivity linearly increases up to 8 mS cm^{-1} at 80 °C. The change in the case of 2G is much smaller, and 1.8 mS cm^{-1} is reached at 80 °C. The strong difference in temperature dependence is due to the different viscosities, see Figure 4b. At 20 °C, the viscosity is 2.8 mPa s for the TMU electrolyte, whereas it is only 1.6 mPa s for the 2G electrolyte. A temperature increase leads to an exponential decay in viscosity which is much stronger in case of the TMU electrolyte, hence being a likely reason for the more strongly increasing conductivity. Note that both solvents differ also strongly in their relative permittivity which is 7.40[20] for 2G and 23.06–23.60[19] for TMU. The density of the different electrolyte solutions is shown in Figure 4c. Both electrolyte solutions show values close to 1 g cm^{-3} at 20 °C, whereas the TMU electrolyte (1.016 g cm^{-3}) is slightly denser than the 2G electrolyte (0.996 g cm^{-3}).

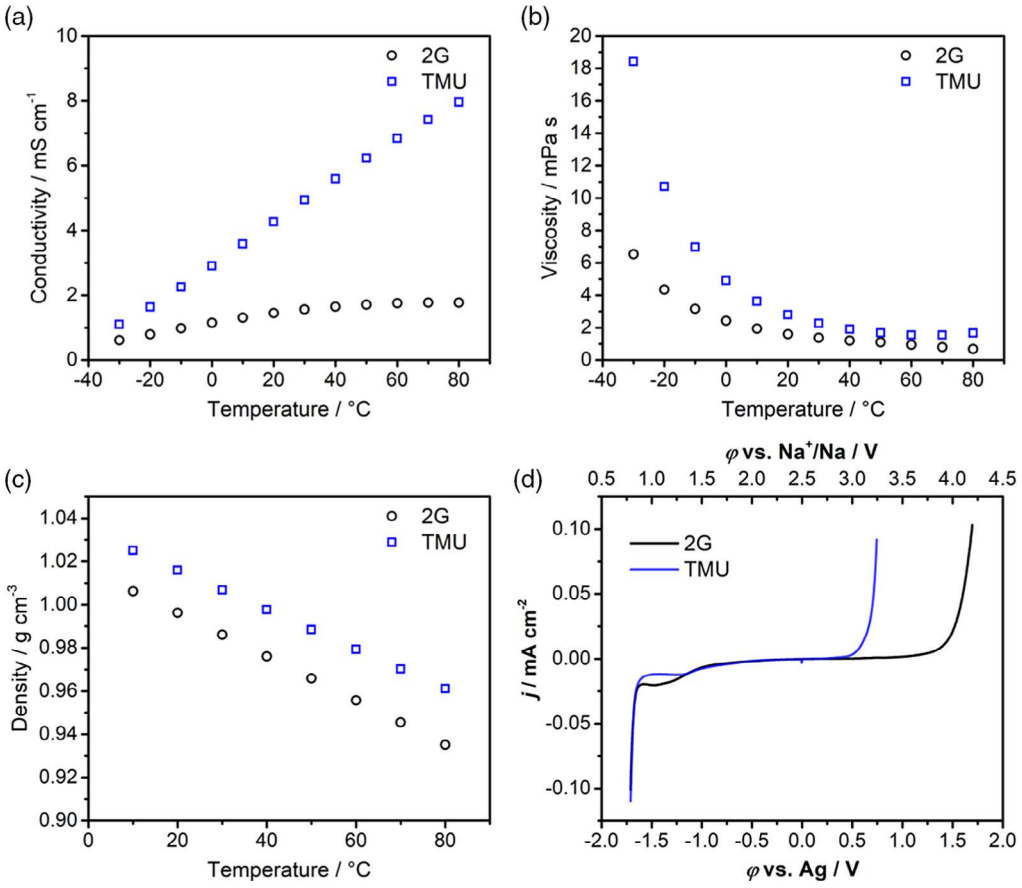

Figure 4. Characterization of TMU and 2G electrolyte containing 0.5 M NaOTf. a) Total ionic conductivity for different temperatures (−30 to +80 °C). b) Viscosity as function of temperature (−30 to +80 °C). c) Density as function of temperature (from +10 to +80 °C). d) LSV curves for ESW determined at 22 °C. A platinum disc was used as a working electrode, activated carbon as a counter electrode, and a silver wire served as quasireference electrode. Potentials were recalculated assuming that the potential of Na^+/Na is −2.5 V relative to the silver quasi-RE.

The ESW of the electrolytes was determined by linear sweep voltammetry (LSV) using platinum as the working electrode, activated carbon as the counter electrode, and silver as the pseudoreference electrode, see Figure 4d and Figure S7, Supporting Information. The reductive stability of both electrolytes is comparable. Reduction starts as early as 1.5 V versus Na^+/Na though major decomposition starts from about 0.8 V versus Na^+/Na. In case of sodium metal as electrode, however, the situation is different. While the 2G-based electrolyte forms a stable SEI,[14] the TMU electrolyte does not and continuous corrosion takes place. For example, exposing a piece of sodium metal to the TMU electrolyte led to complete dissolution within 3 weeks, see Figure S8, Supporting Information. In case of lithium metal, the stability can be improved by mixing TMU with DOL as shown by Zhang et al.[17] However, in case of sodium, TMU is completely incompatible; hence, this solvent cannot be used in the anode compartment of the cell.

Considering the oxidative stability, both electrolytes showed different limiting voltages. While the onset for decomposition of the 2G electrolyte was around 4.0 V versus Na^+/Na, oxidation of the TMU electrolyte started already at around 3.2 V versus Na^+/Na. Although the ESW depends on the type of working electrode used, the results clearly indicate a poorer oxidative stability of the TMU electrolyte, meaning that this solvent can likely not be combined with high-voltage cathodes. However, the redox activity of sulfur and polysulfides takes place at voltages low enough to be in the ESW of the TMU electrolyte. In line with this, we never observed strong side reactions in our Na/polysulfide cell, even though the charging cut-off potential was set to 3.4 V. Note that a three-electrode setup was used for the LSV measurements, whereas the Na/polysulfide cell is a two-electrode setup, which has a large ohmic drop over the liquid/solid electrolyte (electrode distance of 20 mm). Using a Swagelok-type cell, we were able to minimize the ohmic drop and could confirm that the redox activity takes place within the ESW of the TMU electrolyte, see Figure S9, Supporting Information. Nevertheless, as side reactions can be quite subtle, it is clear that future studies should also aim at a more detailed analysis of the ESW in the Na/polysulfide cell. The results of electrolyte characterization at room temperature are shown in **Table 1.**

2.5. Vis Spectroscopy and SOC Determination

Polysulfide-containing solutions can show a different coloration depending on the SOC and the type of solvent used. Vis

Table 1. Properties of the 2G- and TMU-based electrolyte solutions (0.5 M NaOTf). Values for conductivity, viscosity, and density correspond to 20 °C. Electrolyte stability was determined at 22 °C. Permittivity values are taken from given references.

Solvent	Ionic conductivity [mS cm^{-1}]	Viscosity [mPa s]	Density [g cm^{-3}]	Oxidative stability limit [V vs Na^+/Na]	Reductive stability limit [V vs Na^+/Na]	Relative permittivity
2G	1.45	1.603	0.996	4.0	0.8	7.648[22]
TMU	4.27	2.806	1.016	3.2	0.8	23.06–23.60[19]

spectroscopy can therefore be applied to monitor the reaction progress as shown for Li/S cells in tetraglyme or sulfolane electrolyte solutions.[23] In contrast to transition metal complexes that show a different coloration depending on their ligand field configuration, the coloration in case of polysulfides mainly depends on the presence or absence of double-charged polysulfide anions S_x^{2-} or single-charged anion radicals such as $S_3^{-\bullet}$. $S_3^{-\bullet}$-containing solutions are known to absorb visible light in a broad spectrum at around 600 nm, resulting in a characteristic deep blue color.[21,24] As dissolution of polysulfides in the TMU electrolyte leads to a blue coloration, this solvent seems to favor the formation of stable $S_3^{-\bullet}$ radicals. The likely reason for this is the high dipole moment of TMU[17] (3.28–3.66 D[19b]). This would be similar to what has been reported for DMSO-based electrolytes,[21] dimethyl formamide,[25] and hexamethylphosphoramide.[26] In contrast, double-charged (non-radical) polysulfides seem favored in glyme-based electrolytes due to the green, yellow, or also brown coloration.[21,27] Therefore, we assume that oxidation and reduction processes of polysulfides in TMU do not follow the simplified reaction pathways shown in Figure 1b. Instead, the mechanism includes radical oxidation and reduction by single-electron transfer, supporting the suggestions made by Cuisinier et al.[28] and Zhang et al.[17].

Overall, vis spectroscopy is not only a straightforward tool to identify the nature of polysulfide species in different solvents, it can be also used for detecting the SOC of the cell. The latter is difficult otherwise, as the discharge/charge curve of metal–sulfur batteries is often flat.

Figure 5 shows the results from vis spectroscopy experiments on the TMU-based catholyte in which P_2S_5 and Na_2S_5 had been dissolved. For this, aliquots of 3 mL were sampled from the cathode compartment during cycling at different SOC values (Figure S10, Supporting Information**)**. As discussed earlier, a strong absorption band due to $S_3^{-\bullet}$ can be observed around 619 nm. Interestingly, no further signals are visible at lower wavelengths, indicating that almost no long-chain polysulfide dianions are present. The important observation is, however, that only the signal intensity changes during cycling. The peak position and the peak shape remain identical, indicating that $S_3^{-\bullet}$ is the major dissolved species during cell cycling (being in equilibrium with vis-inactive discharge/charge products or some minor component leading to absorbance at a smaller wavelength). Hence, we first focus on the change in absorbance as a function of the SOC. The strongest absorption of 2.75, and hence, the highest $S_3^{-\bullet}$ concentration, was detected for SOC of 45%. Further oxidation directly leads to the formation of optical inactive elemental sulfur and the solution appears nearly transparent in the fully charged state. Reduction, in contrast, should lead to a transparent or yellow solution (Figure S4, Supporting Information). However, discharging is incomplete and after reaching the cut-off potential, still some $S_3^{-\bullet}$ is present. This indicates that the reaction is limited by another process, e.g., electrode passivation or diffusion limitation.

Following the $S_3^{-\bullet}$ signal easily allows following the SOC. However, as the absorbance goes through a maximum at an SOC of 45%, another source of information is needed to determine whether the cell, for a given absorbance, is below or above 45%. For this, we used the weak signal at around 400 nm that appears only when approaching the charged state of the battery. The ratio between the signals at 619 and 400 nm can then be used to determine the SOC, see Figure 5c. Figure 5d shows the vis spectroscopy data of the catholyte solution (SOC = 40%) over 4 days. The absorbance spectra remained identical proving that the solution was stable (within the tested time frame) and side reactions such as disproportionation did not take place. This is again quite different from polysulfides in ether electrolytes as parasitic disproportionation reactions[29] seem to be inhibited or avoided. Therefore, the radical pathway of polysulfide oxidation and reduction might be a relevant factor for the long-term stability of metal–sulfur batteries.

3. Challenges and Future Tasks

The cell concept shown here effectively suppresses any possible cross-talk between both electrodes, which makes it a convenient approach for optimizing the electrolyte compositions for each electrode individually. While the approach is quite promising, we also note some challenges that may serve as a guide for future research directions.

So far, we could cycle our cells only at low absolute currents (2.34 mA) and at a limited polysulfide concentration, amounting to a theoretical cell capacity of 23.4 mAh. The corresponding volumetric capacity was only 0.12 Ah $L^{-1}_{catholyte}$ (≈0.22 Wh $L^{-1}_{catholyte}$). A (too low) concentration of active species is a challenge for many batteries based on soluble electrodes. Future studies therefore have to aim at increasing the catholyte concentration, at least by a factor of 100 to compete with vanadium-based redox-flow technologies (20–70 Wh L^{-1}).[30] Current collectors with a higher surface area and optimized geometry should also improve the cell performance. A more technical task is to reduce the ohmic drop across the cell by reducing the distance of the electrodes. For this, the cell geometry and the implementation of the beta alumina tube must be further optimized. Operating the cell at elevated temperatures is also quite appealing. Unfortunately, our attempts were only partly successful so far. Tests at 60 °C led to issues in the anode compartment (dark coloration of the electrolyte) along with a very

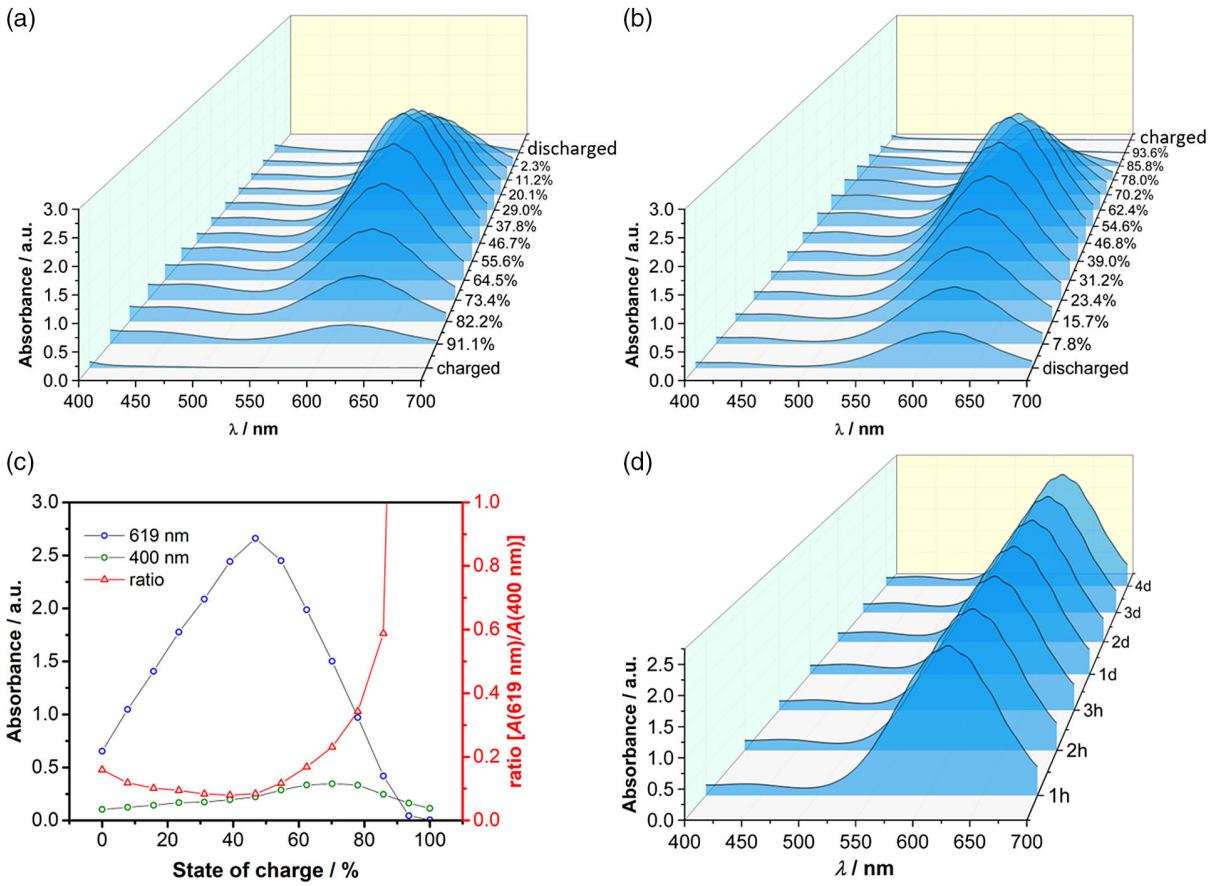

Figure 5. a) Vis spectra of the TMU-based catholyte during cell discharge. The strong absorbance band has a maximum at always 619 nm and represents $S_3^{-\bullet}$ radicals. b) Vis spectra during cell charging. c) Absorbance at 619 and 400 nm as well as their comparison as suggestions for SOC determination. d) Vis spectra of an isolated TMU catholyte at intermediate SOC. No change in absorption behavior over several days reveals that polysulfides are stable. Measured absorbance is given as $\log(I_0/I_T)$. I_0 is the initial light beam intensity, and I_T is the light beam intensity after sample transmission. All spectra were obtained in a two-beam configuration with 0.5 M NaOTf in TMU as reference solution.

erratic discharge/charge behavior, see Figure S11, Supporting Information. Nevertheless, cycling the cell at higher temperatures should be in the focus of future studies. Operating the cell above the melting point of sodium would a) eliminate the need for an anolyte, b) eliminate the issue of dendrite formation, and c) improve the reaction kinetics. We also note that the costs for assembling the cell as shown here are quite high on the laboratory level so far, which limits the number of tests and systematic studies. A practical challenge is also to improve the cell sealing as the performance decreased when operating the cell outside of the glovebox. In light of this, the results shown here should be seen as a proof of concept. The vis spectroscopy measurements are comparably easy to apply; however, we like to point out that the analyzed samples had a maximum active concentration of 1.0 mmol L^{-1} Na_2S_5, equivalent to a maximum $S_3^{-\bullet}$ concentration of 1.67 mmol L^{-1} (if sulfur from P_2S_5 is considered as inactive). The samples had a transmission distance of 9.0 mm; nevertheless, the absorbance value was already almost 3. If vis spectroscopy should be applied for technically more relevant concentrations of >1 mol L^{-1}, very thin transmission distances would be necessary.

4. Conclusions

A sodium polysulfide glass cell was developed in which anode and cathode compartments are separated by a tubular solid electrolyte. The advantage of the cell is that cross-talk between both electrodes is prevented, and the composition of the electrolytes can be optimized for each electrode individually. This also allows to combine a dissolved cathode based on polysulfides (S_x^{2-}) or $S_3^{-\bullet}$ with a solid sodium–metal anode. At the same time, the use of a glass beaker provides an easy way to follow the cell reaction during charging/discharging. While similar cell designs have been suggested and patented earlier, we focused on overcoming present limitations of room-temperature Na–S cells using P_2S_5 as an additive and TMU as an alternative solvent. Starting with a frequently used ether solvent (2G), cell discharge and recharge were very limited due to the formation of solid precipitates. This could be partly alleviated using P_2S_5 as an additive, which leads to transparent solutions and prevention of any visible precipitation. Further and quite significant improvement was obtained by replacing 2G as a catholyte solvent by TMU. The TMU-based catholyte shows clear advantages over 2G in terms

of conductivity, cyclability, and Coulombic efficiency. At current rates of 0.1 C, a specific capacity of more than 800 mAh g_S^{-1} was obtained over 30 cycles without any notable fading. The use of TMU leads to the formation of $S_3^{-\bullet}$ radicals which are present during the complete cell reaction and which can be easily followed by vis spectroscopy as they result into a blue coloration of the catholyte solution. Using vis spectroscopy, the SOC of the battery could be monitored, and the stability of the solution was confirmed. Further studies will be required, however, to further clarify the reaction mechanism in the cathode compartment. The role of phosphorous from the P_2S_5 additive could be investigated by ^{31}P-NMR, for example.

Although challenges and practical hurdles on the lab scale remain, the results of this study show that a careful design of the cell and individual optimization of the electrolyte compositions are effective strategies to further developing low-temperature NaS batteries.

5. Experimental Section

Solid Electrolyte Preparation (Fraunhofer IKTS): Na-β″-alumina ceramics were synthesized by calcining a mixture of AlO(OH) (Nabaltec), Na_2CO_3 (Carl Roth, 99.5% anhydrous), and Li_2CO_3 (Carl Roth, 99%) according to the stoichiometry $Na_{1.67}Al_{10.67}Li_{0.33}O_{17}$ at 1200 °C for 2 h. The obtained white powder was mixed with an organic binder and spray dried into fine granules. The granules were isostatically pressed (2000 bar) into green bodies and sintered under dense MgO crucibles at 1600 °C for 30 min. To calculate the phase composition X-ray diffraction patterns were measured (D8 Advance, Bruker, USA) from a grounded sample and analyzed by Rietveld refinement method (AutoQuan 2.8.0.2). The result is provided in Figure S12 and Table S1, Supporting Information.

Cell Preparation: Most electrochemical cycling results were obtained with a custom-made 200 mL glass beaker-type cell. In addition to the connections for positive and negative electrodes, the steel cap of this cell was equipped with an over-pressure release and an aperture for operando electrolyte sample collection or injection. The sodium electrode was carried by a stainless-steel bolt which was in contact with the cap and located in the center of the cell. This electrode was covered by a Na-β″-aluminate tube (wall thickness = 1 mm, height = 120 mm, and outer diameter = 25 mm), whose inner volume made the anolyte chamber. Anolyte solution was always NaOTf (TCI Chemicals, 98%) dissolved in 2G (Sigma Aldrich, 99.5%) in 0.25–0.5 M concentration. Note that, the conducting salt was purified further by dissolving in boiling ethanol, consecutive filtration, and drying in vacuum at 100 °C for 24 h after solvent removal.

Positive electrode, in contrast, was a carbon paper (GDL H23, Freudenberg) carried by an aluminum ring. In this way, the carbon paper got a cylindrical shape according to the general glass beaker shape. Approximately 32 cm^2 of the carbon dipped into the catholyte solution made of NaOTf (0.5 M), Na_2S_5 (1 mM, BASF), and P_2S_5 (5/3 mM) dissolved in either TMU or 2G for comparison. The anolyte chamber contained 13 mL of electrolyte, whereas the catholyte chamber contained an electrolyte volume of 87 mL. This way the catholyte level was slightly above the liquid level of the anolyte, and the ceramic was gently pushed upward; hence, it did not require further fixation. The catholyte was equipped with a magnetic stirrer.

Additional measurements were carried out in three-electrode Swagelok-type cells. Standard cyclovoltammetry cells contained a 12 mm Na disc as counter electrode and a sodium piece as reference electrode. Both electrodes were in contact with 55 µL electrolyte (0.5 M NaOTf in 2G) and were protected by a Na-β″-aluminate disc (Ionotec) toward preventing polysulfide shuttle and mixing of catholyte and anolyte. One layer of the glass fiber separator (Whatman) was placed between the ceramic and the sodium disc for electrolyte uptake. As the positive electrode, we used two layers of 12 mm GDL H23 carbon fiber soaked in 15 µL of selected electrolyte (0.5 M NaOTf in TMU + 5 mM Na_2S_5 + optionally 8.33 mM P_2S_5).

Cells for conductivity measurements contained two platinum-plated electrodes, no reference, and 450 µL of electrolyte (0.5 M NaOTf in 2G or TMU). The cells were placed inside a climate chamber (Binder) in the purpose of measuring the conductivities by impedance spectroscopy (SP240, Biologic) at different temperatures (0–80 °C).

Swagelok cells for ESW determination at room temperature contained platinum as a working electrode, activated carbon as a counter electrode, and a silver wire as a reference electrode. About 150 µL of electrolyte (0.5 M NaOTf in 2G or TMU) was added onto a glass fiber separator (Whatman) serving as the separator. Separate cells were constructed for oxidation and reduction, respectively. The cells were swept from open-circuit voltage toward either positive or negative direction at 1mV s^{-1} until a current of 10 mA was measured.

All cells were constructed inside an argon-filled glovebox (MBraun) with O_2 and H_2O partial pressure fractions being lower than 0.1 ppm, respectively.

Electrochemical Measurements: Beaker-type cells were electrochemically cycled with an SP150 device (Biologic) in a two-electrode configuration. Galvanostatic measurements were mainly carried out with rather low rates between 0.05 and 0.2 C or accordingly 36 and 144 µA cm^{-2}. The upper voltage limit was 3.4 V, whereas discharge was limited by 1.0 V. Operation took place in the same glovebox where the cells were constructed. Cyclovoltammetry was conducted in a three-electrode configuration with a scan rate of 5 mV s^{-1} up to vertex potential of 3.4 V versus Na^+/Na for oxidation and down to vertex potential of 0.8 V versus Na^+/Na for reduction using an MPG-2 cycler (Biologic) at room temperature.

Vis Spectroscopy: Vis spectra of catholyte solutions were collected with a Perkin Elmer Lambda 35 UV–vis spectrometer (two-beam setup). The scanned wavelength range was 700–400 nm; scan speed was set to 480 nm min^{-1}; and resolution was 1 nm^{-1}. About 3 mL polysulfide solution of a running beaker cell with TMU catholyte was analyzed in defined time intervals of usually 1 h using an air-tight quartz cuvette (d = 9.0 mm). The reference vial was filled with sulfur-free electrolyte. The electrochemical cell operation was paused during vis spectra measurements. To avoid high catholyte volume consumption, analyzed solutions were reinjected into the beaker cell before proceeding with discharge or charge.

Viscosity and Density: The viscosity of the electrolytes was determined using a rheometer MCR 102 (Anton Paar) in the temperature range comprised between −30 and 80 °C. The shear rate for all tests was set to 50 s^{-1}.

The density of the electrolytes was determined in the temperature range comprised between 10 and 80 °C, using a density meter DMA 4100M (Anton Paar).

Supporting Information

Supporting Information is available from the Wiley Online Library or from the author.

Acknowledgements

The authors are grateful to the federal state of Thuringia (*ProExzellenz* program) and the long-term support within the *International Network for Electrochemistry and Batteries* of BASF SE.

Conflict of Interest

The authors declare no conflict of interest.

Keywords

Na/S batteries, P_2S_5 additives, polysulfides, tetramethylurea electrolytes, Vis spectroscopy

Received: October 11, 2019
Revised: December 10, 2019
Published online: January 9, 2020

[1] NGK Insulators, https://www.ngk-insulators.com/en/news (accessed: October 2019).
[2] a) P. Adelhelm, P. Hartmann, C. L. Bender, M. Busche, C. Eufinger, J. Janek, *Beilstein J. Nanotechnol.* **2015**, *6*, 1016; b) S. H. Chung, A. Manthiram, *Adv. Mater.* **2019**, *31*, e1901125; c) D. Kumar, S. K. Rajouria, S. B. Kuhar, D. K. Kanchan, *Solid State Ionics* **2017**, *312*, 8; d) T. Li, J. Xu, C. Wang, W. Wu, D. Su, G. Wang, *J. Alloys Compd.* **2019**, *792*, 797; e) F. Li, Z. Wei, A. Manthiram, Y. Feng, J. Ma, L. Mai, *J. Mater. Chem. A* **2019**, *7*, 9406; f) G. Nikiforidis, M. C. M. van de Sanden, M. N. Tsampas, *RSC Adv.* **2019**, *9*, 5649.
[3] a) T. Cleaver, P. Kovacik, M. Marinescu, T. Zhang, G. Offer, *J. Electrochem. Soc.* **2017**, *165*, A6029; b) S.-H. Chung, C.-H. Chang, A. Manthiram, *Adv. Funct. Mater.* **2018**, *28*, 1801188; c) M. Wild, L. O'Neill, T. Zhang, R. Purkayastha, G. Minton, M. Marinescu, G. J. Offer, *Energy Environ. Sci.* **2015**, *8*, 3477; d) W. Kang, N. Deng, J. Ju, Q. Li, D. Wu, X. Ma, L. Li, M. Naebe, B. Cheng, *Nanoscale* **2016**, *8*, 16541.
[4] L. Medenbach, P. Adelhelm, *Top Curr. Chem.* **2017**, *375*, 81.
[5] L. Medenbach, I. Escher, N. Kowitsch, M. Armbruster, L. Zedler, B. Dietzek, P. Adelhelm, *Angew. Chem., Int. Ed. Engl.* **2018**, *57*, 13666.
[6] a) K. M. Abraham, R. D. Rauh, S. B. Brummer, *Electrochim. Acta* **1978**, *23*, 501; b) R. D. Rauh, K. M. Abraham, G. F. Pearson, J. K. Surprenant, S. B. Brummer, *J. Electrochem. Soc.* **1979**, *126*, 523.
[7] a) S. Wenzel, H. Metelmann, C. Raiß, A. K. Dürr, J. Janek, P. Adelhelm, *J. Power Sources* **2013**, *243*, 758; b) I. Kim, J.-Y. Park, C. H. Kim, J.-W. Park, J.-P. Ahn, J.-H. Ahn, K.-W. Kim, H.-J. Ahn, *J. Power Sources* **2016**, *301*, 332.
[8] a) X. Yu, A. Manthiram, *Chem. Mater.* **2016**, *28*, 896; b) J.-Q. Huang, Q. Zhang, H.-J. Peng, X.-Y. Liu, W.-Z. Qian, F. Wei, *Energy Environ. Sci.* **2014**, *7*, 347; c) I. Bauer, M. Kohl, H. Althues, S. Kaskel, *Chem. Commun.* **2014**, *50*, 3208.
[9] a) F. Yang, S. M. A. Mousavie, T. K. Oh, T. Yang, Y. Lu, C. Farley, R. J. Bodnar, L. Niu, R. Qiao, Z. Li, *Adv. Energy Mater.* **2018**, *8*, 1701991; b) G. Nikiforidis, G. J. Jongerden, E. F. Jongerden, M. C. M. van de Sanden, M. N. Tsampas, *J. Electrochem. Soc.* **2019**, *166*, A135.
[10] N. Li, Z. Weng, Y. Wang, F. Li, H.-M. Cheng, H. Zhou, *Energy Environ. Sci.* **2014**, *7*, 3307.
[11] M. R. Busche, T. Drossel, T. Leichtweiss, D. A. Weber, M. Falk, M. Schneider, M. L. Reich, H. Sommer, P. Adelhelm, J. Janek, *Nat. Chem.* **2016**, *8*, 426.
[12] a) R. Demir-Cakan, *J. Power Sources* **2015**, *282*, 437; b) Y. Jin, G. Zhou, F. Shi, D. Zhuo, J. Zhao, K. Liu, Y. Liu, C. Zu, W. Chen, R. Zhang, X. Huang, Y. Cui, *Nat. Commun.* **2017**, *8*, 462; c) F. Y. Fan, W. C. Carter, Y. M. Chiang, *Adv. Mater.* **2015**, *27*, 5203.
[13] Z. Lin, Z. Liu, W. Fu, N. J. Dudney, C. Liang, *Adv. Funct. Mater.* **2013**, *23*, 1064.
[14] M. Goktas, C. Bolli, J. Buchheim, E. J. Berg, P. Novak, F. Bonilla, T. Rojo, S. Komaba, K. Kubota, P. Adelhelm, *ACS Appl. Mater. Interfaces* **2019**, *11*, 32844.
[15] L. Medenbach, C. L. Bender, R. Haas, B. Mogwitz, C. Pompe, P. Adelhelm, D. Schröder, J. Janek, *Energy Technol.* **2017**, *5*, 2265.
[16] a) Z. Lin, Z. Liu, W. Fu, N. J. Dudney, C. Liang, *Angew. Chem., Int. Ed. Engl.* **2013**, *52*, 7460; b) M. Kohl, F. Borrmann, H. Althues, S. Kaskel, *Adv. Energy Mater.* **2016**, *6*, 1502185; c) J. Pampel, S. Dörfler, H. Althues, S. Kaskel, *Energy Storage Mater.* **2019**, *21*, 41; d) Y. X. Ren, H. R. Jiang, T. S. Zhao, L. Zeng, C. Xiong, *J. Power Sources* **2018**, *396*, 304.
[17] G. Zhang, H. J. Peng, C. Z. Zhao, X. Chen, L. D. Zhao, P. Li, J. Q. Huang, Q. Zhang, *Angew. Chem., Int. Ed. Engl.* **2018**, *57*, 16732.
[18] G. Weddigen, *J. Electrochem. Soc.* **1980**, *127*, 1225.
[19] a) C. Okpala, A. Guiseppi-Elie, D. M. Maharajh, *J. Chem. Eng. Data* **1980**, *25*, 384; b) A. Lüttringhaus, H. W. Dirksen, *Angew. Chem., Int. Ed.* **1964**, *3*, 260.
[20] C. F. Riadigos, R. Iglesias, M. A. Rivas, T. P. Iglesias, *J. Chem. Thermodyn.* **2011**, *43*, 275.
[21] Q. Zou, Y. C. Lu, *J. Phys. Chem. Lett.* **2016**, *7*, 1518.
[22] A. Lago, M. A. Rivas, J. Legido, T. P. Iglesias, *J. Chem. Thermodyn.* **2009**, *41*, 257.
[23] a) C. Barchasz, F. Molton, C. Duboc, J. C. Lepretre, S. Patoux, F. Alloin, *Anal. Chem.* **2012**, *84*, 3973; b) M. U. Patel, R. Demir-Cakan, M. Morcrette, J. M. Tarascon, M. Gaberscek, R. Dominko, *ChemSusChem* **2013**, *6*, 1177; c) X. Yu, A. Manthiram, *J. Phys. Chem. Lett.* **2014**, *5*, 1943.
[24] R. Steudel, T. Chivers, *Chem. Soc. Rev.* **2019**, *48*, 3279.
[25] R. J. H. Clark, D. G. Cobbold, *Inorg. Chem.* **2002**, *17*, 3169.
[26] T. Chivers, I. Drummond, *Inorg. Chem.* **1972**, *11*, 2525.
[27] a) K. H. Wujcik, D. R. Wang, A. Raghunathan, M. Drake, T. A. Pascal, D. Prendergast, N. P. Balsara, *J. Phys. Chem. C* **2016**, *120*, 18403; b) Q. Wang, J. Zheng, E. Walter, H. Pan, D. Lv, P. Zuo, H. Chen, Z. D. Deng, B. Y. Liaw, X. Yu, X. Yang, J.-G. Zhang, J. Liu, J. Xiao, *J. Electrochem. Soc.* **2015**, *162*, A474.
[28] M. Cuisinier, C. Hart, M. Balasubramanian, A. Garsuch, L. F. Nazar, *Adv. Energy Mater.* **2015**, *5*, 1401801.
[29] a) S. S. Zhang, *Electrochim. Acta* **2013**, *97*, 226; b) Y. Chen, H. Zhang, W. Xu, X. Yang, Y. Yu, X. Li, H. Zhang, *Adv. Funct. Mater.* **2018**, *28*, 1704987.
[30] M. Skyllas-Kazacos, G. Kazacos, G. Poon, H. Verseema, *Int. J. Energy Res.* **2010**, *34*, 182.